Transition Metal Chemistry (2021) 46:509–522
https://doi.org/10.1007/s11243-021-00469-1

A polydentate ligand based on 2,2′-dipyridylamine unit linked benzo-15-crown-5; alkali and transition metal complexes; photoresponsive ligand; antimicrobial evaluation against pathogenic microorganisms

Serhat Koçoğlu[1,2] · Zeliha Hayvali[2] · Hatice Ogutcu[3]

Received: 21 March 2021 / Accepted: 22 June 2021 / Published online: 30 June 2021

Abstract

New double-armed benzo-15-crown-5 compound (**L**) was successfully synthesized from 4',5'-bis(bromethyl)benzo-15-crown-5 with 2,2'-dipyridylamine. The synthesized host molecule (**L**), the dipyridylamine unit was able to coordinate Ni^{2+}, Cu^{2+} and Ag^{+} metal cations, whereas the crown ether moiety bound with the alkali metal cations (Na^{+} and K^{+}). The structures of the ligand (**L**), alkali metal complexes (**NaL** and $\mathbf{KL_2}$) and transition metal complexes (**[NiLOAc]**, **[CuLOAc]** and $\mathbf{[AgLNO_3]}$) were characterized by spectroscopic methods. NMR and mass data provided exact evidence of complex formation through both coordination centers of the new ligand (**L**). Both parts (dipyridyl and crown ether) were linked to form a potential fluorescent-sensing compound (**L**) for metal cations. Therefore, to investigate the metal selectivity, different metal cations (Na^{+}, Mg^{2+}, K^{+}, Ba^{2+}, Cr^{3+}, Fe^{3+}, Co^{2+}, Ni^{2+}, Cu^{2+}, Zn^{2+} and Ag^{+}) and the new sensing compound (**L**) fluorescence spectra were recorded. Coordinations with Zn^{2+}, Fe^{3+} and Cu^{2+} induced obvious changes on their increasing concentrations in fluorescence spectra. Crown ethers, as representatives of supramolecular compounds, are also promising antibacterial active compounds because of their ionophoric features. Synthesized ligand (**L**) and complexes (**NaL**, $\mathbf{KL_2}$, **[NiLOAc]**, **[CuLOAc]** and $\mathbf{[AgLNO_3]}$) also proved to be adjuvants that helped to overcome antimicrobial resistance in a range of bacteria and yeast. The antimicrobial activity of compounds was screened in vitro against some pathogenic Gram-positive bacteria, some Gram-negative bacteria and yeast.

Introduction

Crown ether ligands have been extensively studied since their discovery by Pedersen in 1967 and have been used as cation binding subunits in various receptors [1, 2]. They have selectivity for a particular metal cation according to their particular molecular structure. From this perspective, crown ethers have been extensively studied as a host–guest recognition unit in a variety of receptors and applications due to their size differences and strong affinity for metal ions [2, 3]. Armed crown ethers are particularly interesting molecules in supramolecular chemistry. Ditopic crown ethers having binding site for both cation species (alkali and transition) have to be designed to overcome more challenges than just simple metal ion receptors [4].

2,2′-Dipyridylamine is widely used in organometallic and inorganic chemistry as a multidentate ligand [4–6]. The coordination ability of 2,2′-dipyridylamine has been the subject of many studies reflecting its affinity for a number of transition metal ions [7, 8]. Pd^{2+} and Pt^{2+} complexes of 2,2′-dipyridylamine and its derivatives have also been investigated as potential anticancer agents due to their structural similarities to *cis*-platin [9]. A number of new dipyridylamine ligands have been used in studies ranging from cation coordination and supramolecular compounds to the synthesis of new luminescent compounds [6].

In this work we present the synthesis of symmetrical 2,2′-dipyridyl substituted benzo-15-crown-5 core (Scheme 1). This compound with multiple binding sites has

✉ Serhat Koçoğlu
serhatkocoglu@baskent.edu.tr

[1] Food Processing Department, Kahramankazan Vocational School, Başkent University, 06980 Ankara, Turkey

[2] Department of Chemistry, Faculty of Science, Ankara University, 06100 Ankara, Turkey

[3] Department of Field Crops, Faculty of Agriculture, Kırşehir Ahi Evran University, 40100 Kırşehir, Turkey

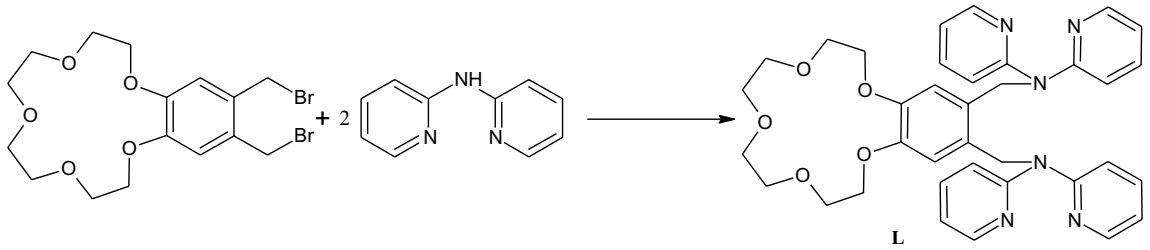

Scheme 1 Proposed structure of new ligand (**L**)

been prepared to improve selective ion sensing. The synthesized new ligand (**L**) has two coordinative binding centre (crown ether cavity and the NN donor atoms of the 2,2′-dipyridyl unit). The crown ether moiety binds alkali metal cations (Na^+ and K^+) and the dipyridyl unit is able to coordinate transition metal cations (Ni^{2+}, Cu^{2+} and Ag^+)

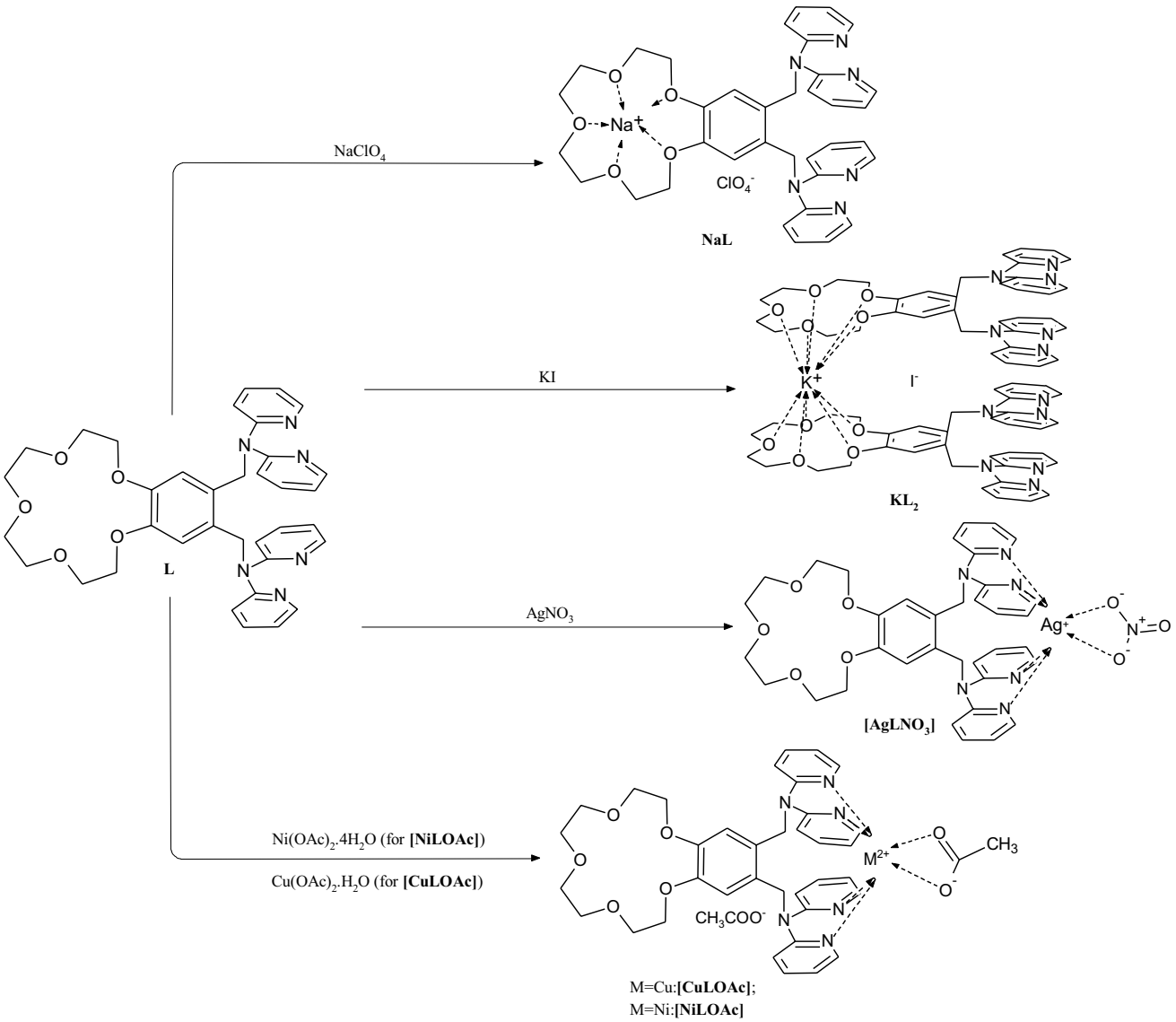

Scheme 2 Proposed structure of new alkali metal complexes (**NaL** and $\mathbf{KL_2}$) and transition metal complexes (**[NiLOAc]**, **[CuLOAc]** and $\mathbf{[AgLNO_3]}$)

(Scheme 2). New alkali and transition metal complexes (**NaL**, **KL_2**, **[NiLOAc]**, **[CuLOAc]** and **[$AgLNO_3$]**) were synthesized and characterized. Different cationic radii and ionic nature lead to the formation of distinct complex structural properties. The details of synthesis and spectral characterization of these compounds are described in the following.

The fluoroionophoric character of the ligand (**L**) was detected by fluorescence spectroscopy. Because the design of multitasking sensors can find different applications in biochemistry and analytical chemistry. For example, they may play an important role in the detection of small amounts of toxic or beneficial metal ions.

The antimicrobial behaviors of the ligand (**L**) and complexes (**NaL**, **KL_2**, **[NiLOAc]**, **[CuLOAc]** and **[$AgLNO_3$]**) were investigated. Because many crown ether compounds and complexes are known to have antimicrobial effects [10]. In terms of antimicrobial activity, one of the most interesting properties of crown ethers is that crown ether behave very similarly to natural ionophores. Since crown ethers clearly distinguish different ions, they can serve as synthetic model compounds suitable for their biological counterparts and may have similar functions. In this study, we observed that a new crown ether ligand and complexes that show significant activity against various microorganisms are more sensitive than standard antibiotics. The compounds differ significantly in their activity against the microorganisms tested, pointing to differences in cell walls between Gram-positive and Gram-negative bacteria.

Experimental

Physical measurements

All commercially available solvents and reagents were used as obtained by Sigma-Aldrich Chemical Company unless otherwise stated. Alkali metal cations were added to the solution as fluorescence reagents in the form of iodide and other metal cations were added as metal nitrate salts. All of the reactions were monitored by thin layer chromatography using fluorescent material coated silica sheets (Merck 60 PF-254). Starting compounds (tetraethylene glycol dichloride [11] benzo-15-crown-5 [1] and 4',5'-bis(bromomethyl) benzo-15-crown-5 [12]) were synthesized according to the literature. Melting points were determined on a Gallenkamp melting point platform. ^{1}H- and ^{13}C-NMR spectra were detected on a Varian Mercury, High Performance Digital FT-NMR (400 MHz) spectrometer ($SiMe_4$ as an internal standard; chemical shifts: ppm (δ)). The IR spectra were recorded using a Shimadzu IRAffinity-1 model FTIR spectrometer equipped three reflections ATR attachment. Mass spectral analyses were performed on an Agilent Technologies 6224 TOF LC/MS spectrometer. Fluorescence spectra were recorded on a Perkin Elmer LS-50B Fluorescence Spectrometer.

Test microorganisms

The pathogenic bacterial cultures; *Staphylococcus aureus* ATCC25923, *Escherichia coli* ATCC1280, *Salmonella typhi* H NCTC901.8394, *Staphylococcus epidermis* ATCC12228, *Micrococcus luteus* ATCC9341, *Bacillus cereus* RSKK-863, *Klebsiella pneumonia* ATCC 27,853*, Proteus vulgaris* RSKK 96,026, *Listeria monocytogenes* 4b ATCC19115, *Serratia marcescens* sp.*, Shigella dysenteria* type 2 NCTC2966 and yeast were used *Candida albicans* Y-1200-NIH.

Detection of antimicrobial activity

The synthesized compounds were examined for their antimicrobial activity by the well-diffusion method against Gram-negative bacteria, Gram-positive bacteria and one yeast [13, 14].

All of the compounds were kept dry at room temperature and dissolved (10^3 µM) in DMSO. DMSO has been used as a solvent both for compounds and also for control and it was found to have no antimicrobial activity against any of the microorganisms. 1% (v/v) of 24 h broth culture (pathogenic bacteria and yeast) containing 10^6 CFU/mL were placed in sterile petri. Mueller- Hinton Agar (MHA) (15 mL) kept at 45 °C was then poured into the petri plate and allowed to solidity. Then wells of 6 mm diameter were punched attentively by using a sterile cork borer and were entirely loaded with the new compounds. In the last stage, petri plates were incubated for 24 h at 37 °C on the incubator. On completion of the incubation period, the mean value obtained for the two wells were used to calculate the zone of growth inhibition of each sample The pathogenic bacterial cultures and yeast were tested for resistance to five antibiotics (Ampicillin, Nystatin, Kanamycin, Sulphamethoxazol, Amoxycillin) produced by Oxoid Lt., Basingstoke, UK [15, 16].

Synthesis of new ligand (L)

The 2,2'-dipyridylamine (0.34 g, 2.0 mmol) was dissolved in DMSO (50 mL). KOH (0.11 g, 2.0 mmol) was added in small amounts and the resulting reaction mixture was refluxed for 1 h. Subsequently, 4',5'-bis(bromomethyl) benzo-15-crown-5 (0.45 g, 1.0 mmol) in DMSO (20 mL) was added dropwise to the reaction mixture. The resulting solution was refluxed for 10 h then the complete consumption of the starting material was observed by TLC (silica, eluent; THF). Then, water was added until the solution turned cloudy. The yellow precipitate formed was isolated

and recrystallized from hexane. Yield 0.21 g (33%), mp 85 °C.

Synthesis of sodium and potassium complexes (NaL and KL_2)

The new crown ether ligand (**L**) (0.128 g, 0.2 mmol) and $NaClO_4$ (0.024, 0.2 mmol) or KI (0.017 g, 0.1 mmol) were dissolved in dry EtOH (10 mL) and heated to reflux for 2 h. The precipitated complex was filtered and washed with diethyl ether. Yield 0.034 g (22%). mp 108 °C (for **NaL**) and Yield 0.065 g (45%), mp 132 °C (for $\mathbf{KL_2}$).

Synthesis of Ni(II) and Cu(II) complexes ([NiLOAc], [CuLOAc])

To a solution of crown ether ligand (**L**) (0.064 g, 0.1 mmol) in methanol (10 mL) at room temperature was added a solution of $Ni(OAc)_2.4H_2O$ (0.025 g, 0.1 mmol) or $Cu(OAc)_2.H_2O$ (0.020 g, 0.1 mmol) in methanol (5 mL) with stirring. The mixture was refluxed for 2 h and the mixture was allowed to cool to room temperature. Then the mixture was filtered and dried in vacuum. Yield 0.025 g (33%), mp 130 °C (for **[NiLOAc]**) and Yield 0.027 g (36%), mp 97 °C (for **[CuLOAc]**).

Synthesis of Ag(I) complex ([$AgLNO_3$])

To a solution of crown ether ligand (**L**) (0.064 g, 0.1 mmol) in dichloromethane/methanol 1:1 (10 mL) at room temperature was added a solution of $AgNO_3$ (0.017 g, 0.1 mmol) in methanol (5 mL) with stirring. The mixture was refluxed for 2 h and the mixture was allowed to cool to room temperature. Then the mixture was filtered and dried in vacuum. Yield 0.047 g (58%) mp 138 °C.

Results and discussion

Synthesis and structural characterisations

The synthesis phase of this study consists of two parts. The first part is the synthesis of the new double-armed crown ether ligand (**L**), which is a tetradentate ligand. The second part of the study includes complexation studies of alkali (Na^+ and K^+) and transition metal cations (Ni^{2+}, Cu^{2+} and Ag^+) with new ligand (**L**).

New crown ether compound (**L**) was obtained from the reaction of the starting compound 4′,5′-bis-(bromomethyl)-benzo-15-crown-5 and 2,2′-dipyridylamine in DMSO with KOH (Scheme 1).

Alkali metal complexes (**NaL** and $\mathbf{KL_2}$) were prepared from ligand (**L**) with $NaClO_4$ or KI in ethanol solution. The alkali metal cation inclusion complexes analysis indicates that the ligand (**L**) is favorable for binding the Na^+ and K^+ and the O-M (M = Na^+ and K^+) interaction has a ion–dipole interactions [17, 18]. Na^+ ion is compatible the cavity of benzo-15-crown-5 in complex well and thus is just accommodated in the crown ring to form 1:1 metal:ligand complex [19]. In general, the K^+ ion does not fit well into the benzo-15-crown-5 space in the complex and therefore is placed between the two crown ether rings, forming a 1: 2 metal: ligand sandwich complex [17, 20, 21]. ^{1}H-NMR and mass spectral data confirmed the proposed structures.

In the transition metal complexation reactions with nickel(II), copper(II) and silver(I), sudden color changes were observed with the addition of metal salt in reaction mixture (yellow to olive green for nickel complex, petroleum green for copper complex and brown for silver complex). This is the first sign that the ligand interacts with the metal cation and complexes are formed. The Ni(II), Cu(II) and Ag(I) ions are further surrounded by four nitrogen atoms of the ligand and acetate anion (for nickel and copper complexes) and nitrate anion (for silver complex). The obtained complexes were analyzed with IR, ^{1}H-NMR, ^{13}C-NMR and HRMS techniques. Particularly, NMR and HRMS spectral data provided evidence for the structural characterizations and coordinations of new complexes.

Mass spectra

The HRMS mass spectra of ligand (**L**) and complexes (**NaL**, $\mathbf{KL_2}$, **[NiLOAc]**, **[CuLOAc]** and **[$\mathbf{AgLNO_3}$]**) were recorded. All of the compounds examined provided nice quality mass spectra and the molecular ion peaks and molecular weight of the ligand and complexes have been confirmed. Mass spectral data (found and calculated molecular ion peaks and error ratios of the compounds) are summarized in (Table 1).

The molecular ion peak $[M+H]^+$ at m/z 635.29927 supports the proposed structure of the ligand (**L**) (Fig. 1).

Mass spectra of the alkali metal complexes (**NaL** and $\mathbf{KL_2}$) indicated that the sodium complex was 1:1 (metal:ligand) and the potassium complex was 1:2 (metal:ligand), sandwich complex (Fig. 1). According to the literature, the complexation of the benzo-15-crown-5 with Na^+ cations can be called "filling complexes" [22, 23]. The molecular ion peak $[M+Na]^+$ of the sodium complex was detected at m/z 657.277738. For K^+ complex, the molecular ion peak correspond to the $[2\,M+K]^+$ and obtained at m/z 1307.54213. The potassium cation is located between two crown ether cavity such as sandwich (Scheme 2).

Mass spectra provided crucial evidence for the structure of transition metal complexes (**[NiLOAc]**, **[CuLOAc]** and **[$\mathbf{AgLNO_3}$]**) (Fig. 1). In the mass spectrum of Ni(II) complex (**[NiLOAc]**), the molecular ion peak was detected at m/z 751.23571 and correspond to the ligand plus nickel

Table 1 Mass spectral data (in CH_3CN)

Compound	Molecular ion peak	Mass (found $gmol^{-1}$)	Mass (calculated $gmol^{-1}$)	Tolerance (ppm)
L	$[M+H]^+$	635.29927	635.29822	−1.65
NaL	$[M+Na]^+$	657.277738	657.28016	3.68
KL_2	$[2\,M+K]^+$	1307.54213	1307.54450	1.81
[NiLOAc]	$[M+Ni+COOCH_3]^+$	751.23571	751.23906	4.46
	$[M+2+Ni+COOCH_3]^+$	753.23387	753.23450	0.84
[CuLOAc]	$[M+Cu+COOCH_3]^+$	756.22870	756.23331	6.10
	$[M+2+Cu+COOCH_3]^+$	758.22873	758.23150	3.65
$[AgLNO_3]$	$[M+Ag+NO_3+Na]^+$	826.17272	826.17310	0.46
	$[M+2+Ag+NO_3+Na]^+$	828.17286	828.17275	−0.13
	$[M+Ag+NO_3+K]^+$	842.14583	842.14704	1.44
	$[M+2+Ag+NO_3+K]^+$	844.14635	844.14669	0.40
	$[M+Ag]^+$	741.19459	741.19549	1.21
	$[M+2+Ag]^+$	743.19496	743.19514	0.24

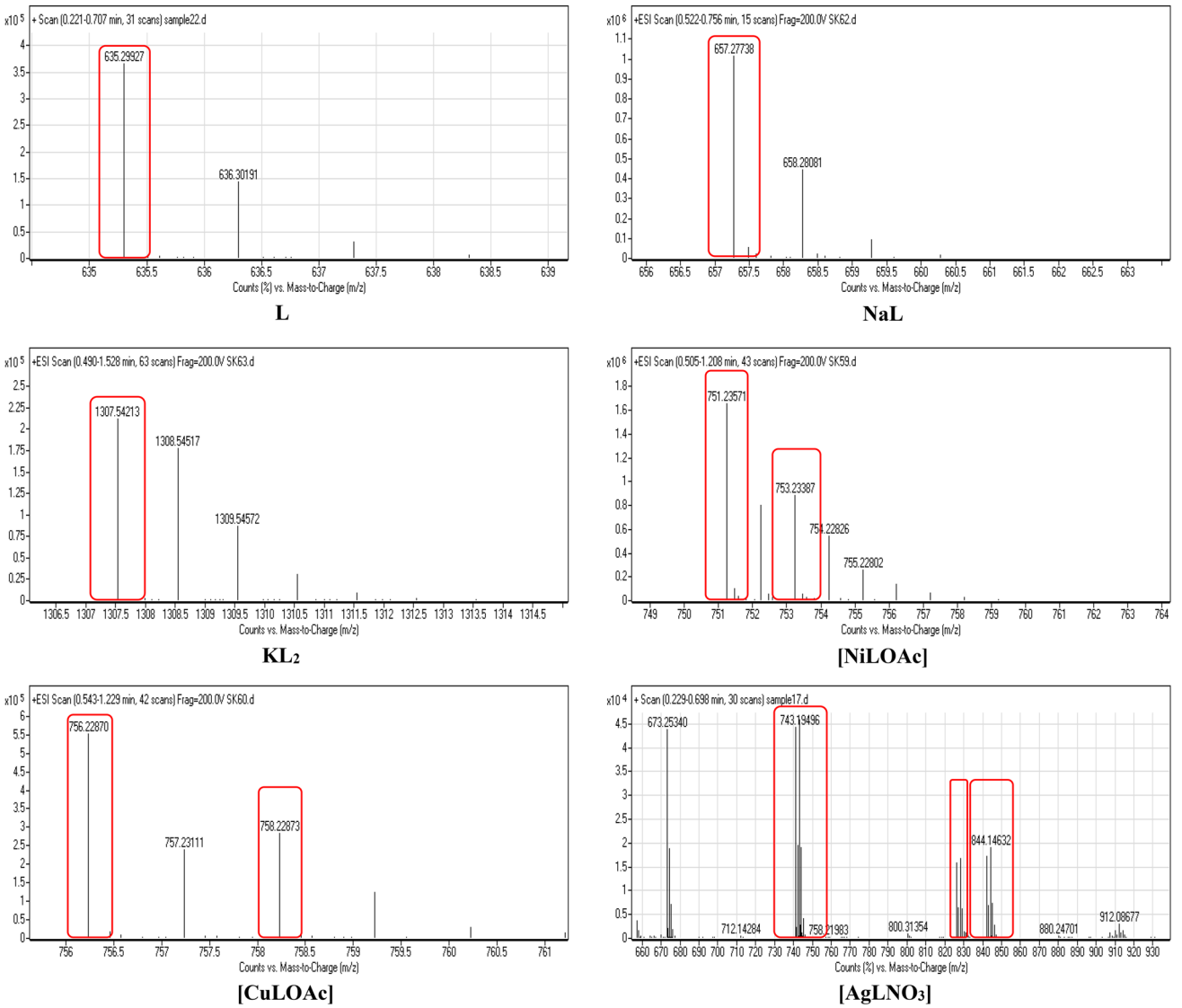

Fig. 1 The mass spectra of ligand (**L**) and its metal complexes (**NaL**, **KL_2**, **[NiLOAc]**, **[CuLOAc]** and **$[AgLNO_3]$**)

acetate ($[M+Ni+CH_3COO]^+$). The molecular ion peak of the complex supports the proposed structure. In the mass spectrum of Cu(II) complex (**[CuLOAc]**), the molecular ion peak was detected at m/z 756.22870 and correspond to the ligand plus copper acetate ($[M+Cu+CH_3COO]^+$). The Ni(II) and Cu(II) complexes have the isotope peaks of the M and M + 2 from the nickel(II) and copper(II) atoms (%68.08 ^{58}Ni, %26.22 ^{60}Ni and %69.17 ^{63}Cu, %30.83 ^{65}Cu) (Fig. 1). The observation of the molecular ion peak, which also contains the acetate anion in the mass spectra, suggested that the Ni(II) and Cu(II) complexes formed were six-coordinated (Scheme 2). In the mass spectrum of the Ag(I) complex (**[AgLNO$_3$]**), two corresponding molecular ion peaks of $[M+Ag+NO_3+Na]$ and $[M+Ag+NO_3+K]$ were detected. Seeing molecular ion peaks where sodium and potassium ions adducts to the structure is quite common in HRMS-TOF spectra [24, 25]. The spectrum shows that the M and M + 2 peaks at m/z 826.17272 and 828.17286 (for $[M+Ag+NO_3+Na]^+$) and 842.14583 and 844.14635 (for $[M+Ag+NO_3+K]^+$) complexes, respectively (Supplementary Fig. S1). A ratio of the peaks is 1:1 as expected for silver(I) isotope (%51.84 ^{107}Ag, %48.16 ^{109}Ag) peak patterns. In addition, the dominant peak in *m/z* 743.19496 is the fragmentation pattern of the complex (**[AgLNO$_3$]**) and corresponds to the ligand plus silver(I) ($[M+Ag]^+$). Mass spectrum data suggested that the Ag(I) complex formed a six-coordinated structure with 2,2'-dipyridyl N atoms and nitrate anion (Scheme 2).

FTIR spectra

Selected IR data for the ligand (**L**) and complexes (**NaL**, **KL$_2$**, **[NiLOAc]**, **[CuLOAc]** and **[AgLNO$_3$]**) are given in Table 2. The aliphatic $\upsilon_{(C\text{-}H)}$ vibrations for **L** were observed in the range of 2926–2870 cm^{-1}. The aromatic and aliphatic $\upsilon_{(C\text{–}O\text{–}C)}$ vibrations appeared between 1269–1238 and 1126–1107 cm^{-1}, respectively. The IR spectrum of the ligand (**L**) shows characteristic internal $\upsilon_{(C=N)}$ absorption bands at 1582, 1371 cm^{-1} (C-N stretching).

The IR spectra of the ligand (**L**) and alkali metal complexes (**NaL** and **KL$_2$**) were almost of the same frequency. The anion ClO_4^- in sodium complex (**NaL**) gives rise to IR absorption bands at 1080 cm^{-1} and 617 cm^{-1}. These bands attributable to the asymmetric υ_{as}(Cl-O) stretching band (1080 cm^{-1}) and the asymmetric υ_{as}(O-Cl-O) bending band (617 cm^{-1}), suggesting that both bounded and uncoordinated free ClO_4^- are present. In the spectrum of the ligand (**L**), three peaks were recorded at 978, 883 and 937 cm^{-1}. The two peaks at 978 and 883 cm^{-1} were observed as smaller peaks in alkali metal complexes (**NaL** and **KL$_2$**) than in ligand (**L**). This is an evidence that there is a conformational changes in the crown ether ring during the complexation [15, 26].

The IR spectra of the transition metal complexes (**[NiLOAc]**, **[CuLOAc]** and **[AgLNO$_3$]**) were compared with that of the free ligand (**L**) to determine the changes that might have taken place during the complexation. Due to the bending of the acetate (OC = O) group in the spectra of the **[NiLOAc]** and **[CuLOAc]** complexes, new peaks were observed at 659, 648 cm^{-1} (for Ni^{2+} complex) and 673, 651 cm^{-1} (for Cu^{2+} complex). In addition, changes were observed in the peaks ranging from 1580 to 1450 cm^{-1}. These changes are believed to be due to the effect of the ligand and acetate coordinated with the metal cation. FTIR can be useful to probe the coordination between acetate and metal cations [27, 28]. Acetate may be a bidentate ligand where both oxygen atoms bond to the metal cation, so metal's coordination number was six. The six coordination sites were distributed between 2,2'-dipyridyl N atoms and acetato in a neutral way as in complexes (**[NiLOAc]**, **[CuLOAc]**), as shown in Scheme 2. The Cu(II) ion in complex was proposed to have a distorted octahedral environment. If the acetate was a monodentate ligand, one of the oxygen would bind to the metal while the other would remain a double bond (C = O)

Table 2 Selected IR bands of ligand and complexes (ν cm^{-1})

Compound	ν(C = C)	ν(C = N)	ν_{as}(C–O–C)$_{arom}$	ν(C-H)$_{aliph}$	ν_{as}(C–O–C)$_{aliph}$	ν_s(C–O–C), ν_{as}(C–C), $\nu_{rocking}$(CH_2)	M-OAc
(L)	1512;1466(m)	1582;1371(m)	1269;1238(s)	2926;2870(w)	1126;1107(s)	978, 883, 937	–
(NaL)[a]	1512;1466(m)	1582;1373(m)	1242(s)	2924;2878(w)	1080(s)	–, –, 941	–
(KL_2)	1512;1466(s)	1582;1373(s)	1234(s)	2924;2870(w)	1103(s)	–, –, 933	–
[NiLOAc]	1514;1466(m)	1582;1373(m)	1265;1238(m)	2922;2870(w)	1126;1096(s)	978, 883, 937	659, 648
[CuLOAc]	1514;1466(s)	1582;1381(m)	1269;1238(m)	2926;2870(w)	1126;1096(s)	978, 883, 935	673, 651
[$AgLNO_3$][b]	1508;1468(m)	1585;1366(s)	1273;1230(s)	3005;2970(w)	1160(s)	949, 893, 910	–

[a]strong peak at $\nu(ClO_4^-)$: 1080 cm^{-1} and 617 cm^{-1}; [b]coordinated nitrate anion at 1386 cm^{-1} and 1321 cm^{-1}

w: weak; m: medium; s: strong

and a sharp peak of 1590–1650 cm^{-1} would be expected to be observed in the spectrum [29].

The IR spectrum of the Ag(I) complex is quite different than ligand spectrum. Several large changes occur in the spectra of complex, in particular the 1585–1321 cm^{-1} region. New peaks (709 cm^{-1}, 669 cm^{-1}) occurring at lower frequencies in the spectrum of the complex (**[AgLNO$_3$]**) are likely due to Ag^+-nitrogen bonds. Very strong bands corresponding to the NO_3^- stretch of the coordinated nitrate anion were detected at 1386 cm^{-1} and 1321 cm^{-1} [30].

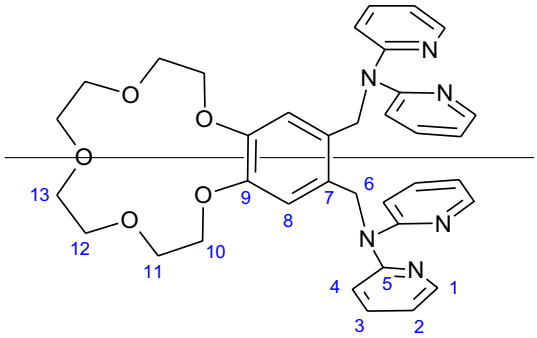

Scheme 3 Numbering scheme of ligand (**L**)

^{1}H- and ^{13}C-NMR Spectra

The ligand (**L**) and complexes (**NaL**, **KL$_2$**, **[NiLOAc]**, **[CuLOAc]** and **[AgLNO$_3$]**) ^{1}H-NMR spectral data are summarized in Table 3. The synthesized molecules are symmetric, so the number of aliphatic and aromatic proton peaks were made taking into account the half of the molecule. Numbering scheme of the **L** is given in Scheme 3. Five different aromatic protons ($H_{1\text{-}4,\ 8}$) expected to be observed in the ^{1}H-NMR spectrum of **L** were recorded as multiplet peaks (only H_8 proton peak as a singlet) in the range at δ = 6.84–8.33 ppm. Each peak of the aromatic protons was determined separately and given in Table 3. The peaks of the 15-crown-5 protons (-OCH_2-CH_2O-) were detected to resonate between δ = 3.56–3.79 ppm. In addition, aliphatic H_6 proton peak was detected as a singlet at 5.55 ppm (Supplementary Fig. S2).

The ^{1}H-NMR spectra of the alkali metal complexes (**NaL** and **KL$_2$**) are very similar to the ligand spectrum, but some differences still provide evidence that sodium and potassium complexes are formed (Supplementary Fig. S3 and Fig. S4). Different peak shapes and multiples were observed in the ^{1}H-NMR spectra of alkali metal complexes. Since the complexing directly affects the crown ether ring, especially the crown ether proton (-OCH_2CH_2O-) peak region had a very different peak multiplets [15, 17] (Fig. 2). Although sharp three peaks were seen for the ligand (**L**), four peaks were observed for the sodium complex (**NaL**) and distinct peak multiplets for the potassium complex (**KL$_2$**) at crown ether proton peaks region.

One-dimensional ^{1}H NMR spectroscopy was also unsuccessful to determine whether the Ni(II), Cu(II) and Ag(I) species were complex coordination in solution, but supportive information was obtained about coordination numbers and metal:ligand ratio by HRMS analysis. The six-coordinate functionalized complexes (**[NiLOAc]**, **[CuLOAc]** and **[AgLNO$_3$]**) were prepared by the condensation of tetradentate crown ether ligand donor atoms and CH_3COO^- (for **[NiLOAc]** and **[CuLOAc]**) or NO_3^- (for **[AgLNO$_3$]**). The above-mentioned facts showed that ligand (**L**) can coordinate with nickel(II), copper(II) and silver (I) ion as in Scheme 2. ^{1}H NMR studies have been carried out to characterize these paramagnetic nickel(II) and copper(II) complexes in solution (Supplementary Figs. S5 and S6). The magnetic moment of paramagnetic metal ions generally causes very effective nuclear magnetization relaxation in neighboring nuclei, causing broad NMR signals [31, 32]. The slow electronic relaxation of paramagnetic Ni(II) and

Table 3 H^1-NMR spectral data of the ligand (**L**) and metal complexes (**NaL**, **KL$_2$**, **[NiLOAc]**, **[CuLOAc]** and **[AgLNO$_3$]**) (δ, ppm)

Compound	H1	H2	H3	H4	H6	H8	H10	H11	H12	H13	-CH_3
L	8.31 (d; 4H)	6.86 (t; 4H)	7.52 (t; 4H)	7.16 (d; 4H)	5.53 (s; 4H)	6.81 (s; 2H)	3.79 (t, 4H)	3.64 (t; 4H)	3.56 (m; 8H)		–
NaL	8.33 (dd; 4H)	6.88 (m; 4H)	7.55 (m; 4H)	7.15 (d; 4H)	5.54 (s; 4H)	6.90 (s; 2H)	3.89 (t, 4H)	3.78 (t; 4H)	3.71 (t; 4H)	3.65 (t; 4H)	–
KL_2	8.30 (dd; 8H)	6.87 (dd; 8H)	7.54 (m; 8H)	7.20 (d; 8H)	5.54 (s; 8H)	6.82 (s; 4H)	3.68 (m, 8H)	3.40 (m; 8H)	3.30 (m; 8H)	3.25 (m; 8H)	–
[NiLOAc]	8.31 (m; 4H)	6.87 (t; 4H)	7.54 (m; 4H)	7.16 (m; 4H)	5.52 (s; 4H)	6.80 (s; 2H)	3.80 (m; 4H)	3.65 (m; 4H)	3.58 (m; 8H)		2.59 (s; 3H)
[CuLOAc]	8.31 (m; 4H)	6.85 (m; 4H)	7.51 (m; 4H)	7.15 (m; 4H)	5.52 (s; 4H)	6.81 (s; 2H)	3.81 (m; 4H)	3.65 (m; 4H)	3.58 (m; 8H)		2.60 (s; 3H)
[$AgLNO_3$]	8.33 (m; 4H)	6.90 (t; 4H)	7.61 (m; 4H)	7.04 (d; 4H)	5.57 (s; 4H)	6.49 (s; 2H)	3.78 (m; 4H)	3.72 (m; 4H)	3.65 (m; 8H)		–

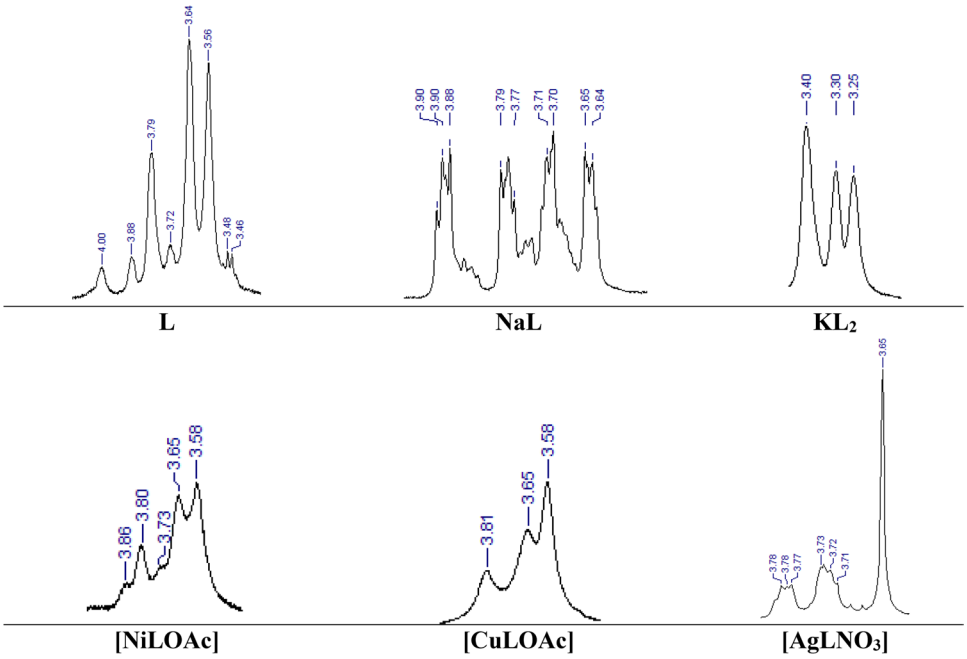

Fig. 2 ^{1}H-NMR spectra of the crown ether protons (-OCH-$_2$CH$_2$O-) peak region; in $CDCl_3$

Cu(II) ions usually results in broad line widths and poor resolution of the NMR spectra, which makes their interpretation very difficult, if not impossible [33]. The paramagnetic nickel(II) and copper(II) complexes (**[NiLOAc]** and **[CuLOAc]**) exhibit extremely broader ^{1}H NMR signals but expected proton peaks were detected (Table 1). Crown ether proton (H_{10}-H_{13}) peaks in the ^{1}H-NMR spectrum of the Ni(II) complex (**[NiLOAc]**) were observed as broad multiplet peaks in the range of 3.58–3.80 ppm. Aliphatic H_6 proton peak was detected as singlet peak at 5.52 ppm, while aromatic proton peaks (H_2-H_5 and H_8) were observed as broad multiplets (Supplementary Fig. S5). The ^{1}H-NMR spectrum of the copper(II) complex (**[CuLOAc]**) spectrum is similar to the nickel(II) complex spectrum (Supplementary Fig. S6). Aliphatic H_6 proton peak was detected as singlet peak at 5.52 ppm, while aromatic proton peaks (H_2-H_5 and H_8) were observed as broad multiplets. Crown ether proton peaks (H_{10}-H_{13}) were detected in the range of 3.58–3.81 ppm as expected. Depending on the diamagnetic Ag(I) atom, sharp peaks were detected in the ^{1}H-NMR spectra of the Ag(I) complex (**[AgLNO$_3$]**), unlike the Ni(II) and Cu(II) complexes (**[NiLOAc]** and **[CuLOAc]**) (Supplementary Fig. S7). Crown ether proton (H_{10}-H_{13}) peaks in the ^{1}H-NMR spectrum of the Ag(I) complex were observed as multiplets at 3.65–3.78 ppm. Aliphatic H_6 and aromatic H_8 proton peaks were detected as singlet peak at 5.57 ppm and 6.49 ppm while aromatic proton peaks (H_2-H_5) were observed as multiplet peaks.

The ^{13}C-NMR spectral data for the ligand (**L**) have been assigned and are given in Table 4. All of the carbons in the

Table 4 C^{13}-NMR spectral data of the ligand (**L**) and metal complexes (**NaL**, **KL$_2$**, **[NiLOAc]**, **[CuLOAc]** and **[AgLNO$_3$]**) (δ, ppm)

Compound	C1	C2	C3	C4	C5	C6	C7	C8	C9	C10-C13	-CH_3
L	148.19	117.27	137.33	114.65	157.10	48.14	129.61	113.50	146.93	68.11; 68.72; 69.13; 69.70	–
NaL	147.97	117.43	137.66	114.57	156.55	47.49	129.11	113.16	146.42	68.07; 68.20; 69.03; 69.53	–
KL_2	147.96	117.41	137.64	114.55	156.55	47.49	128.98	113.08	146.40	67.93; 68.04; 68.98; 69.48	–
[NiLOAc]	147.84	117.30	137.53	114.46	156.44	47.37	128.73	113.02	146.48	68.12; 68.24; 69.31; 69.81	47.72
[CuLOAc]	147.15	117.80	138.08	115.40	156.20	47.79	129.27	113.66	146.11	68.76; 68.88; 69.94; 70.45	48.50
[$AgLNO_3$]	148.26	117.77	138.07	115.05	156.63	47.81	128.51	113.43	146.72	68.25; 68.39; 69.48; 70.00	–

^{13}C-NMR spectrum indicates the molecule to be symmetric (Scheme 3). The peaks of the eight 15-crown-5 carbons are observed between δ = 68.11–69.70 ppm. The peaks for the aliphatic and aromatic carbons were observed in the corresponding region.

When the ^{13}C-NMR spectra of the ligand and alkali metal complexes were compared, very small and significant changes were observed in crown ether -OCH_2CH_2O- peaks, as referenced by several previous works [24, 25]. Very low chemical shifts are generally observed in sodium complexes, especially in the region of aromatic and crown ether carbons. In the complex (**NaL**) spectrum, the signals of crown ether carbons shifted to slightly lower ppm and were detected between 67.93–69.70 ppm. The peaks of the all aromatic carbons were observed in the expected region and were equal to the number in the proposed structures.

^{13}C-NMR spectra of transition metal complexes (**[NiLOAc]**, **[CuLOAc]** and **[AgLNO$_3$]**) showed eight aromatic carbon signals. -OCH_2CH_2O- carbons were observed in the expected region as four peaks due to the symmetrical structure. When the ligand (**L**) spectrum and the spectra of the complexes (**[NiLOAc]**, **[CuLOAc]** and **[AgLNO$_3$]**) were compared, it was observed that the aliphatic C6 carbon peak shifted to the lower field (47.37, 47.94 and 47.81 ppm, respectively). Similarly, C5 carbons (for complexes) were observed in the region of 156.44, 155.43 and 156.63 ppm and showed a lower field shift compared to the ligand (**L**). In ^{13}C-NMR spectra of Ni(II) and Cu(II) complexes the peak at 47.72 and 48.50 ppm were observed belonging to the -CH_3 carbon of the CH_3COO^- group.

Optical characteristics

The fluorescence emission studies were performed by preparing the ligand (**L**) solution at a concentration of 5×10^{-5} M in EtOH. To examine the metal selectivity of synthesized ligand (**L**), different cations (Na^+, Mg^{2+}, K^+, Ba^{2+}, Cr^{3+}, Fe^{3+}, Co^{2+}, Ni^{2+}, Cu^{2+}, $Zn^{2+}$and Ag^+) were added to the ligand (**L**) (Fig. 3).

The ligand (**L**) fluorescent spectrum showed that the addition of Fe^{3+} and Cu^{2+} quenched the fluorescence (Fig. 3) [34]. Meanwhile, the weak fluorescence emission was recorded with the addition of Cr^{3+} cation. Short wavelength shifts were observed with the addition of Zn^{2+}, Ni^{2+} and Ag^+ at the same concentration to the ligand solution, suggesting that the coordination bonds between metal atoms and 2,2′-bipyridine nitrogen atoms were formed (Fig. 3). As a result of the addition of Na^+, K^+, Mg^{2+} and Ba^{2+} cations to the ligand solution, no noticeable shifts were observed in the spectra at 377 nm, while an increase or decrease in peak intensities was observed. This situation suggested that the metal cations were complexed from the crown ether moiety of the ligand (**L**). The ligand was titrated with Zn^{2+},

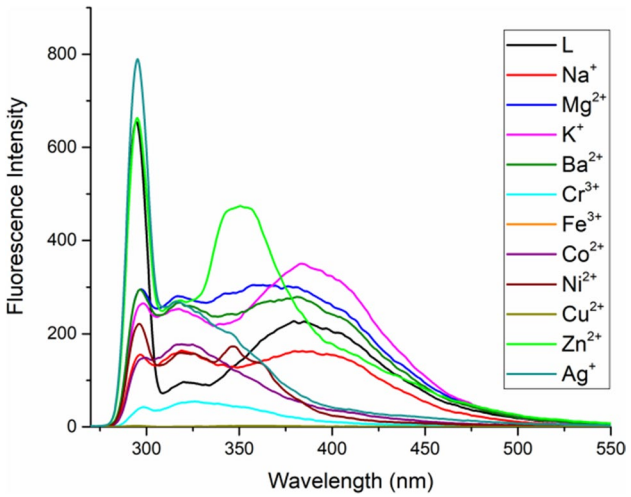

Fig. 3 The effect of metal cations on the fluorescence spectra of **L**; metal salts anion: Na^+ and K^+: I^-; others: NO_3^-; 25 °C; λ_{exc}: 292 nm; ligand concentration *c*: 5×10^{-5} M; metal concentrations *c*: 5×10^{-3} M in EtOH

Fe^{3+} and Cu^{2+} in EtOH and the changes they made in their fluorescence spectra were examined depending on their increasing concentrations (Fig. 4a, b and c). The addition of $Zn(NO_3)_2$ resulted in a larger hypsochromic shift of the emission spectrum than did other metal cations. We have shown that crown ether-substituted bipyridine ligand is suitable for the detection of Zn^{2+} by fluorescence. The emission intensity was also very sensitive to the number of equivalents of Zn^{2+}, with very slight changes occurring upon the addition of 1 to 100 equivalents of the cation (Fig. 4c).

Antibacterial activities

All of the compounds were screened antimicrobial activities against selected pathogenic microorganisms (bacteria and yeast) by the well-diffusion method.

All synthesized compounds exhibited varying degrees of inhibitory effects on the growth of different tested pathogenic bacteria and yeast (Table 5, Figs. 5, 6 and 7). In *L. monocytogenes* all compounds showed approximately inhibition activity to all of the standard antibiotics tested. This pathogen is the causative agent of listeriosis, the leading cause of death among food-borne bacterial pathogens [35, 36].

B. cereus is an opportunist pathogen associated with foodborne diseases [14, 37]. Compound **[AgLNO$_3$]** exhibited the same level of inhibition activity as K30 (28 mm) against *B.cereus*. Compound **L** (25 mm) showed the same inhibition activity as a standard antibiotic SXT25 (25 mm) and higher activity than standard antibiotics AMP10 and AMP30 (23 mm, 20 mm, respectively). Compound **KL$_2$** showed same activity as AMP10 (23 mm) and higher

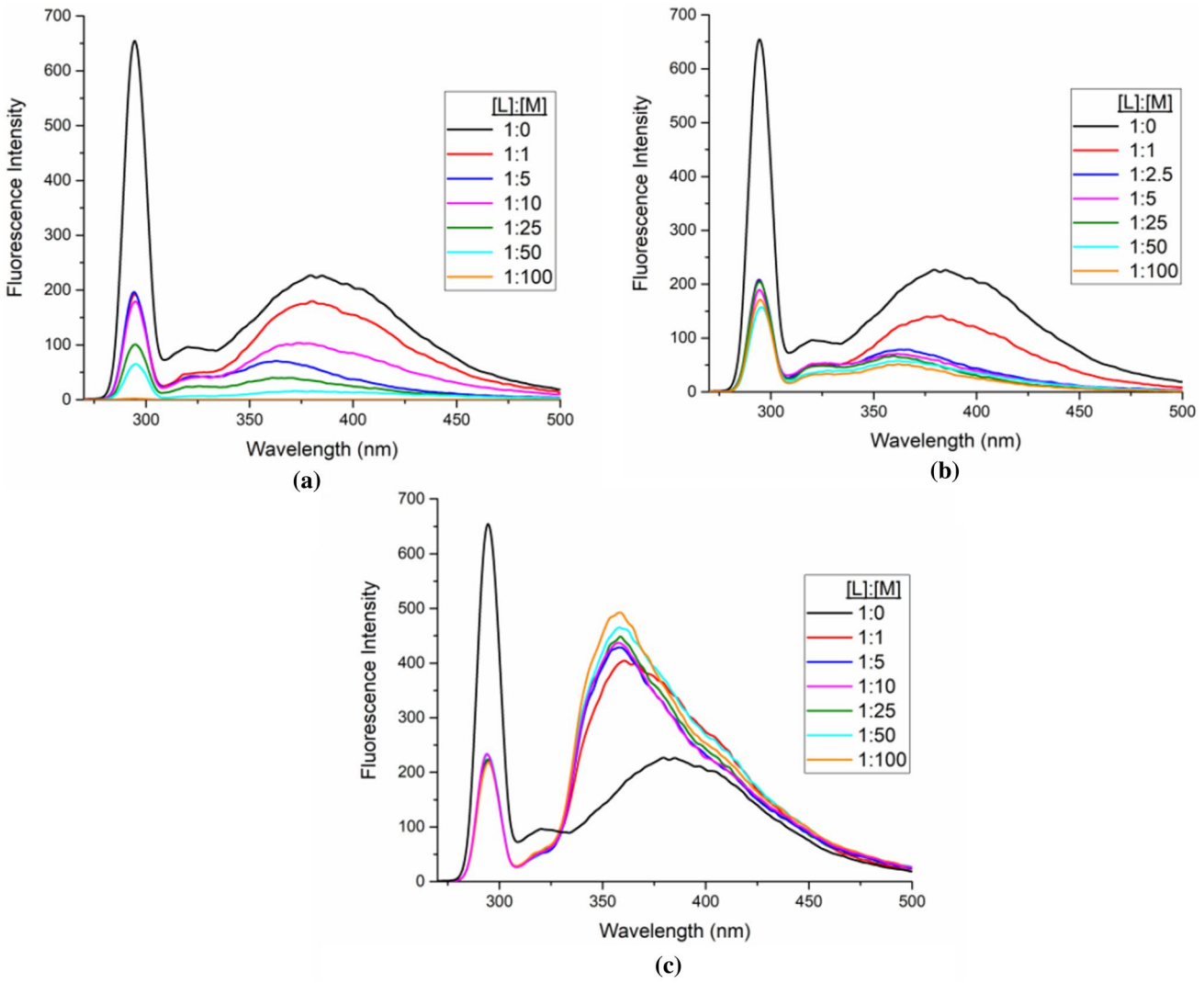

Fig. 4 The fluorescence spectral changes of **L** during the addition of 1–100 equivalent of **a** Fe^{3+}; **b** Cu^{2+}; **c** Zn^{2+}. 25 °C; λ_{exc}: 292 nm; ligand concentration *c*: 5×10^{-5} M; metal concentration *c*: 5×10^{-3} M in EtOH

Table 5 Antimicrobial activity of new compounds (**L**, **NaL**, **KL_2**, **[NiLOAc]**, **[CuLOAc]** and **[$AgLNO_3$]**) and standard reagents

Microorganisms		Compounds						Standart antibiotics				
		L	NaL	KL_2	[NiLOAc]	[CuLOAc]	[$AgLNO_3$]	K30	SXT25	AMP10	AMC30	NYS100
Gram (+)	*L.monocytogenes*	20	21	20	20	20	22	26	25	28	23	–
	S.epidermis	25	20	18	18	-	20	27	24	15	27	–
	S.aureus	–	–	-	-	-	19	25	24	30	30	–
	M.luteus	–	18	25	-	-	25	22	20	16	18	–
	B.cereus	25	17	23	19	-	28	28	25	23	20	–
Gram (-)	*S.typhi H*	20	15	17	16	20	25	20	17	11	19	–
	E.coli	20	20	18	21	22	20	25	18	10	14	–
	K. pneumonia	22	–	-	11	15	13	23	20	21	21	–
	P. vulgaris	15	15	15	20	20	15	21	19	17	20	–
	S. marcescens	22	21	18	16	16	17	–	–	–	–	–
	S. dysenteria 2	–	–	–	17	–	–	–	–	–	–	–
Yeast	*C. albicans*	35	40	34	30	30	36	–	–	–	–	20

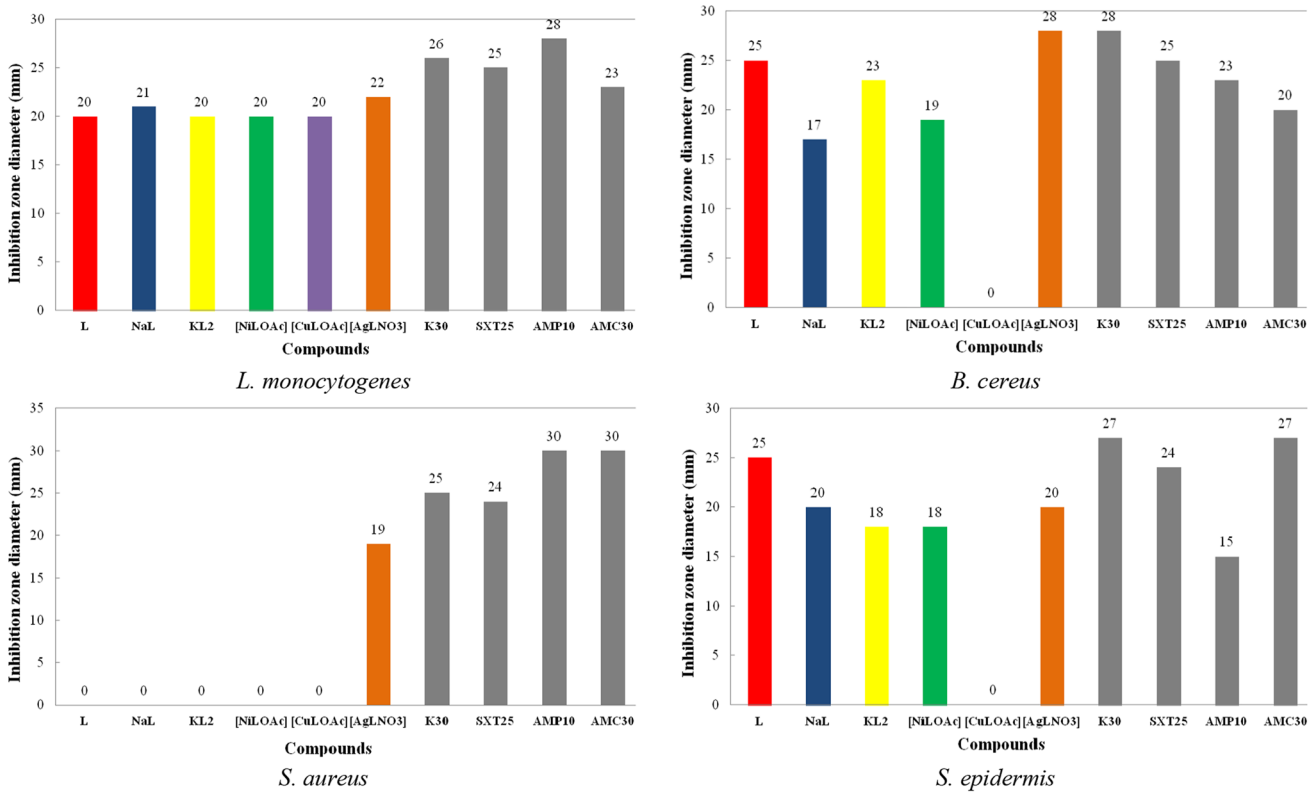

Fig. 5 Antimicrobial activity of new compounds (**L**, **NaL**, **KL_2**, **[NiLOAc]**, **[CuLOAc]** and **[$AgLNO_3$]**) for *L. monocytogenes*, *B. cereus*, *S. aureus* and *S. epidermis* and standard reagents

inhibition activity than standard antibiotic AMC30 (20 mm) (Supplementary Fig. S8).

Compound **L** (25 mm) showed higher inhibition effect than standard antibiotics SXT25 (24 mm) and AMP10 (15 mm) against *S. epidermis*. Further compounds **NaL**, **[$AgLNO_3$]**, **KL_2** and **[NiLOAc]** (20 mm, 20 mm, 18 mm, 18 mm respectively) showed better activity than the standard antibiotics AMP10 (15 mm) against *S.epidermis*.

M. luteus has considered an opportunistic pathogen that can be responsible for nosocomial infections. Moreover, it can cause skin infections and septic shock in immuno compromised patients [38, 39]. Compounds **KL_2** and **[$AgLNO_3$]** (25 mm) showed higher inhibition activity against *M.luteus* than all standard antibiotics tested.

Salmonella serovars cause many different clinical symptoms, ranging from asymptomatic infection to severe typhoid-like syndromes in infants or in some high-sensitivity animals [40]. Compound **[$AgLNO_3$]** (25 mm) showed higher inhibition activity against *S.typhi* H than all standard antibiotics tested. In addition, compounds **L** and **[NiLOAc]** showed same level of inhibition activity as standard antibiotics K30 (20 mm) and higher inhibition activity than standard antibiotic SXT25, AMP10, AMC30 (17 mm, 11 mm, 19 mm respectively) against this important pathogen *Salmonella typhi* H (Supplementary Fig. S9).

In the case of *E.coli*, all compounds (**L**, **NaL**, **KL_2**, **[NiLOAc]**, **[CuLOAc]**, **[$AgLNO_3$]**; 20 mm, 20 mm, 18 mm, 21 mm, 22 mm, 20 mm, respectively) showed rather highly inhibition activity than the standard antibiotics except K30 (25 mm).

In *K. pneumonia*, compound **L** (22 mm) showed better inhibition activity than the standard antibiotics except K30 (23 mm). Further, all compounds showed moderate activity against *Serratia marcencens*.

Systemic fungal infections (including *C. albicans*) have emerged as significant causes of mortality and morbidity in immuno compromised patients (organ or ligament transplantation, cancer chemotherapy, adjuvants) [41, 42]. All the compounds showed much inhibition activity against this yeast (Table 5, Fig. 6). Further, compounds **NaL** and **[$AgLNO_3$]** (40 mm and 36 mm, respectively) showed the most inhibition activity against *C. albicans* as compounds with zone values of 30 mm—40 mm. Sodium complex (**NaL**) (40 mm) showed the highest activity. In fact, all the synthesized compounds showed more activity against *C. albicans* than commercial (standard) antifungal (positive control NYS100P) (Supplementary Fig. S9).

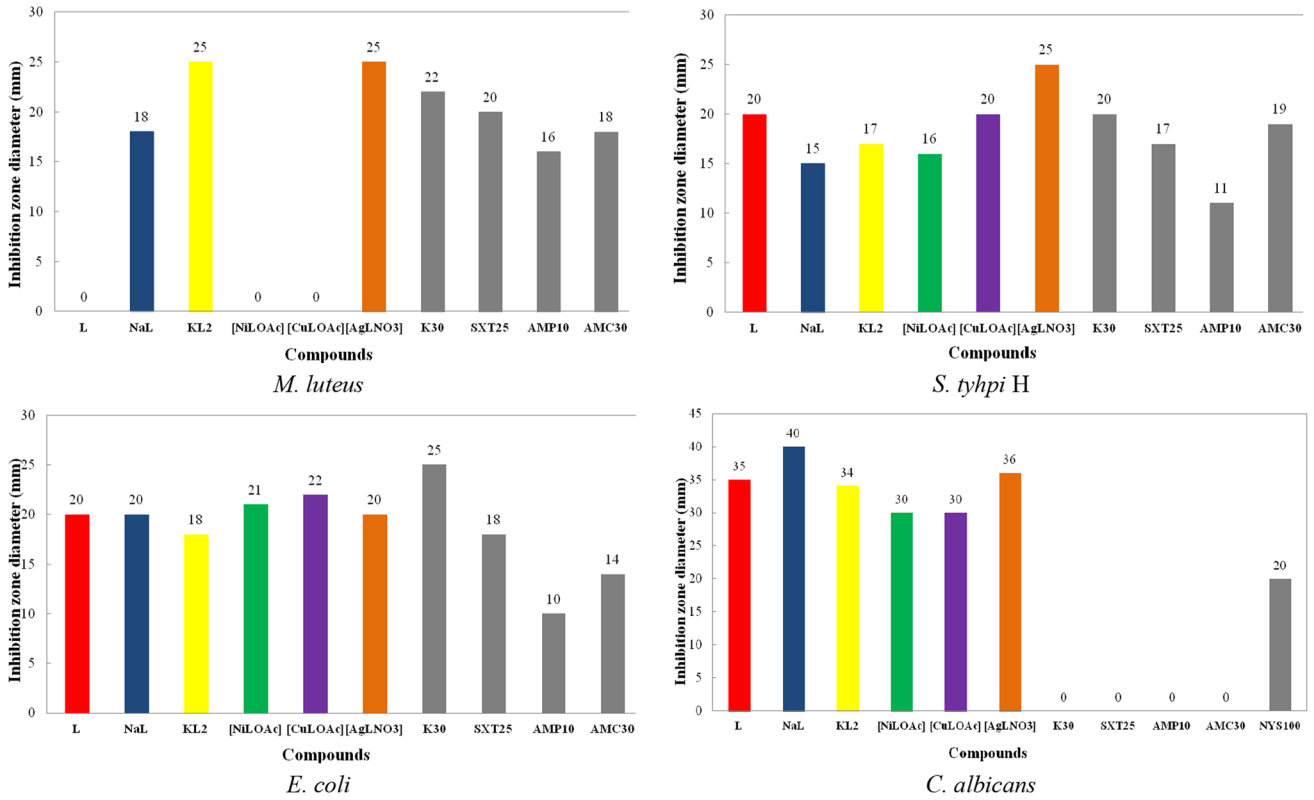

Fig. 6 Antimicrobial activity of new compounds (**L**, **NaL**, **KL_2**, **[NiLOAc]**, **[CuLOAc]** and **$[AgLNO_3]$**) for *M. luteus*, *S. tyhpi* H, *E. coli* and *C. albicans* and standard reagents

The antibacterial activity of these compounds was compared with commercial antibiotics and anticandidal (Ampicillin, Nystatin, Kanamycin, Sulphamethoxazol and Amoxycillin). New compounds showed that greater inhibitory effects on the growth of different tested both pathogenic gram negative, gram positive bacteria and yeast. These inhibition activities may be explained on the basis of Chelation theory [43]. Also **$[AgLNO_3]$** was found to be the higher level of inhibition activity against both Gram(-) and Gram(+) pathogenic bacteria. All compounds showed that greater inhibition activity in Gram-positive bacteria than Gram-negative. Microbiologists agree that Gram-negative bacteria have specialized mechanisms for the extracellular extrusion of strange substances (efflux bomb), limiting the access of antimicrobial agents to the active site. As a result, it prevents the accumulation of antibiotics in the cell and prevents the effect of antimicrobial agents [44].

Conclusion

In this research, new ligand (**L**) and their alkali metal and transition metal complexes (**NaL**, **KL_2**, **[NiLOAc]**, **[CuLOAc]** and **$[AgLNO_3]$**) were synthesized and characterized. Both alkali metal complexes (**NaL** and **KL_2**) have 1:1 and 1:2 (metal:ligand) ratio, respectively. Transition metal complexes (**[NiLOAc]**, **[CuLOAc]** and **$[AgLNO_3]$**) have octahedral geometries with N_4O_2 coordination environment.

We have investigated the fluorescence properties of 2,2'-bipyridine substituted crown ether ligand (**L**) with different metal cations (Na^+, Mg^{2+}, K^+, Ba^{2+}, Cr^{3+}, Fe^{3+}, Co^{2+}, Ni^{2+}, Cu^{2+}, $Zn^{2+}$and Ag^+). The fluorescence response for **L** was selective over other metal cations of Zn^{2+}. As a result, we conclude that the new ligand (**L**) is suitable and photoresponsive for the detection of Zn^{2+} by fluorescence.

Synthesized compounds (**L**, **NaL**, **KL_2**, **[NiLOAc]**, **[CuLOAc]** and **$[AgLNO_3]$**) have been found to exhibit antibacterial and antifungal activities at moderate to good levels both Gram positive, Gram negative bacteria and yeast. The antimicrobial activity results of the compounds were also compared with commercial (standard) antibiotics. It was seen that new compounds were effective as the antibiotics and antifungal mentioned. Anticandidal assays of the free ligand and the complexes show that the complexes, especially **NaL**, is effective against most of the *C. albicans*. In addition, the complex **$[AgLNO_3]$** showed significant antimicrobial activity (*S. typhi* H) compared with a standard antibiotic. These results will inspire us to design new antibacterial and anticandidal reagents containing crown ether for diseases.

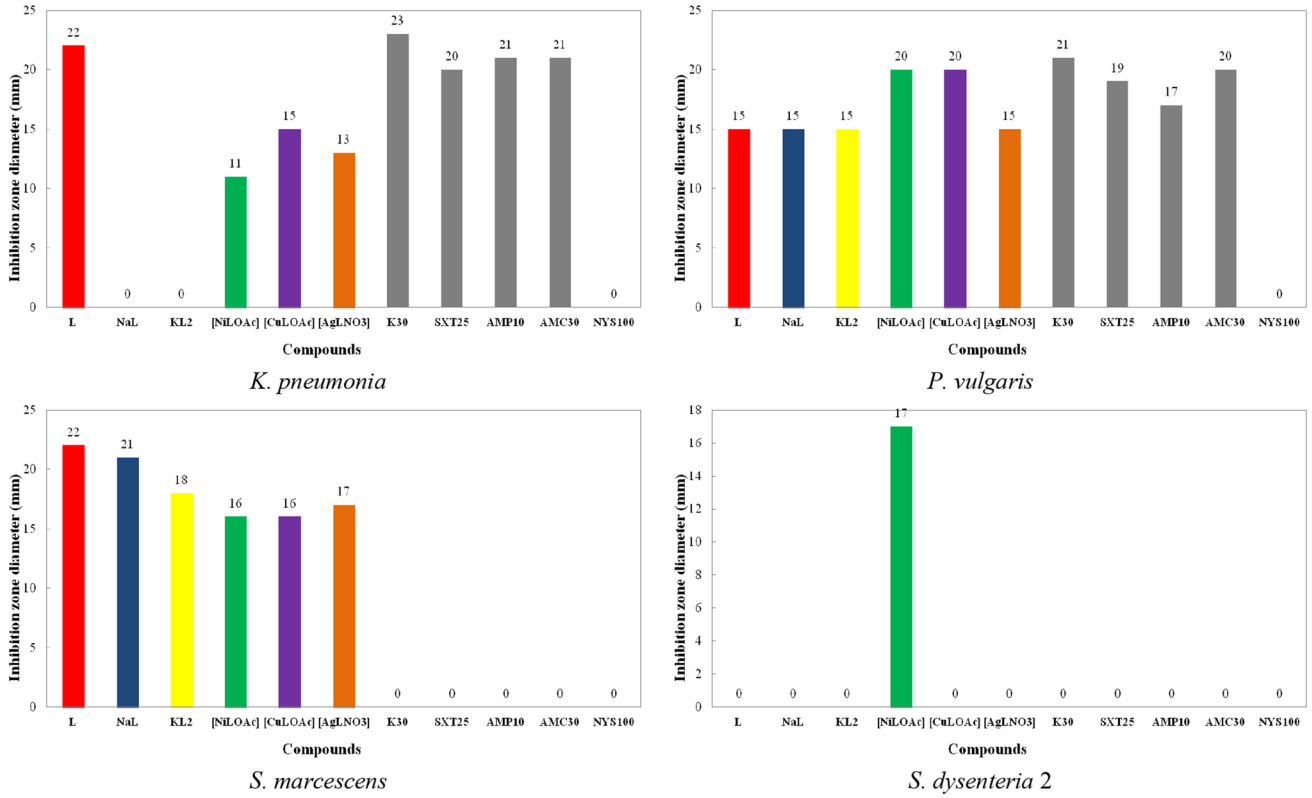

Fig. 7 Antimicrobial activity of new compounds (**L**, **NaL**, **KL_2**, **[NiLOAc]**, **[CuLOAc]** and **[$AgLNO_3$]**) for *K. pneumonia*, *P. vulgaris*, *S. marcescens* and *S. dysenteria* 2 and standard reagents

Supporting information

Mass spectra, ^{1}H-NMR spectra and antimicrobial activity of some compounds are provided as supplementary material.

Supplementary Information The online version contains supplementary material available at https://doi.org/10.1007/s11243-021-00469-1.

Acknowledgements The authors gratefully acknowledge the financial assistance of the Scientific and Technical Research Council of Turkey (TUBITAK), grant No: TBAG 210T122 and Ankara University grant No: 17B0430004.

Declarations

Conflict of interest All authors declare that they have no conflict of interest in this work.

References

1. Pedersen CJ (1967) J Am Chem Soc 89:7017–7036
2. Gokel GW, Leevy WM, Weber ME (2004) Chem Rev 104:2723–2750
3. Li J, Yim D, Jang WD, Yoon J (2017) Chem Soc Rev 46:2437–2458
4. Roelens S, Vacca A, Venturi C (2009) Chem Eur J 15:2635–2644
5. Antonioli B, Bray DJ, Clegg JK, Gloe K, Gloe K, Kataeva O, Lindoy LF, McMutrie JC, Steel PJ, Sumby CJ, Wenzel M (2006) Dalton Trans 40:4783–4794
6. Wu F, Tong H, Wang K, Wang Z, Li Z, Zhu X, Wong WY, Wong WK (2016) J Photochem Photobiol A 318:97–103
7. Youngme S, Chaichit N, Pakawatchai C, Booncoon S (2002) Polyhedron 21:1279–1288
8. Youngme S, Chaichit N, Koonsaeng N (2002) Inorg Chim Acta 335:36–42
9. Rauterkus MJ, Fakih S, Mock C, Puscasu I, Krebs B (2003) Inorg Chim Acta 350:355–365
10. Kralj M (2008) Tušek-Božić, Frkanec L. ChemMedChem 3:1478–1492
11. Calverly MJ, Dale J (1982) Acta Chem Scand 36B:241–247
12. Winkler B, Mau AWH, Dai L (2000) Phys Chem Chem Phys 2:291–295
13. Nithya C, Gnanalakshmi B, Pandian SK (2011) Mar Environ Res 71:283–294
14. Çiçek İ, Tunç T, Ogutcu H, Abdurrahmanoglu S, Günel A, Demirel N (2020) Chemistry Select 5:4650–4654
15. Koçoğlu S, Ogutcu H, Hayvalı Z (2019) Res Chem Intermed 45:2403–2427
16. Karakılıç E, Baran Ş, Öğütçü H, Akdemir A, Baran A (2020) *rac*- and *meso*-Cyclohexanoids: Their α-, β-glycosidases, antibacterial, antifungal activities and molecular docking studies. Arch Pharm. https://doi.org/10.1002/ardp.201900267
17. Liu Y, Han JR, Zhang HY (2004) Supramol Chem 16:247–254

18. Hayvali Z, Gündüz N, Kilic Z, Weber E (2000) Z Naturforsch 55b:975–981
19. Burlov AS, Tsukanov AV, Borodkin GS, Revinskii YV, Dubonosov AD, Bren VA, Garnovskii AD, Tsivadze AY, Minkin VI (2006) Russ J Gen Chem 76:992–996
20. Hayvalı Z, Köksal P (2013) J Incl Phenom Macrocycl Chem 76:369–378
21. Biernat JF, Cygan A, Luboch E, Simonov YA, Malinovski TI (1993) Bel'skii VK, Bolotina NF. J Inclus Phenom Mol 15:369–383
22. Şahin Gül D, Ogutcu H, Hayvalı Z (2020) J Mol Struct 1204:127569
23. Gao Y, Zhong RL, Xu HL, Sun SL, Su ZM (2015) RSC Adv 5:30107–30119
24. Keller BO, Sui J, Young AB, Whittal RM (2008) Anal Chim Acta 627:71–81
25. Tong H, Bell D, Tabei K, Siegel MM (1999) J Am Soc Mass Spectrom 10:1174–1187
26. Ghildiyal N (2017) nee Pant GJ, Rawat MSM, Singh K. Spectrochim Acta A 171:507–514
27. Alcock NW, Tracy VM, Waddington TC (1976) J Chem Soc Dalton Trans 21:2243–2246
28. Mathey Y, Greig DR, Shriver DF (1982) Inorg Chem 21:3409–3413
29. Wang AQ, Golden TD (2013) Int J Electrochem 2013:1–10
30. Zhongy DC, Chen ZF, Liu YC, Luo XJ, Barta C, Liang H (2010) J Coord Chem 63:3146–3154
31. Sánchez-Méndez A, Benito JM, de Jesús E, de la Mata FJ, Flores JC, Gómez R, Gómez-Sal P (2006) Dalton Trans 45:5379–5389
32. Ramadan S, Hambley TW, Kennedy BJ, Lay PA (2004) Inorg Chem 43:2943–2946
33. Koval IA, van der Schilden K, Schuitema AM, Gamez P, Belle C, Pierre JL, Luken M, Krebs B, Roubeau O (2005) Reedijk. J Inorg Chem 44:4372–4382
34. Şahin D, Yılmaz H, Hayvalı Z (2016) Res Chem Intermed 42:6337–6350
35. Sarı N, Şahin SÇ, Öğütcü H, Dede Y, Yalçın S, Altundas A, Doğanay K (2013) Spectrochim Acta A 106:60–67
36. Ramaswamy V, Cresence VM, Rejitha JS, Lekshmi MU, Dharsana KS, Prasad SP, Vijila HM (2007) Microb Infect 40:4–13
37. Ceker S, Ogutcu H, Meral S, Agar AA, Agar G (2019) Pak J Pharm Sci 32:2679–2686
38. Altundas A, Sarı N, Colak N, Ögütcü H (2010) Med Chem Res 19:576–588
39. Nartop D, Hasanoğlu Özkan E, Gündem M, Çeker S, Ağar G, Öğütcü H, Sarı N (2019) J Mol Struct 1195:877–882
40. Nartop D, Demirel B, Güleç M, Hasanoğlu Özkan E, Kurnaz Yetim N, Sarı N, Çeker S, Öğütcü H, Ağar G (2020) Novel polymeric microspheres: Synthesis, enzyme immobilization, antimutagenic activity and antimicrobial evaluation against pathogenic microorganisms. J Biochem Mol Toxic. https://doi.org/10.1002/jbt.22432
41. Nartop D, Sarı N, Öğütcü H (2014) Chin J Inorg Chem 30:921–929
42. Çınarlı M, Yüksektepe Ataol Ç, Bati H, Güntepe F, Ögütçü H, Büyükgüngör O (2019) Inorg Chim Acta 484:87–94
43. Mishra L, Singh VK (1993) Indian J Chem 32A:446–449
44. Reichling J, Koch C, Stahl-Biskup E, Sojka C, Schnitzler P (2005) Rev Bras Ciên Vet 18:62–66